Power-Efficient Protection With Directed p-Cycles for Asymmetric Traffic in Elastic Optical Networks

Min Ju, *Student Member, IEEE*, Fen Zhou, Shilin Xiao, and Zuqing Zhu, *Senior Member, IEEE*

***Abstract*—In this paper, we investigate power-efficient directed preconfigured cycles (p-Cycles) for asymmetric traffic protection in elastic optical networks (EONs) against single link failure. Owing to the advantage of distinguishing traffic amount in two directions, directed p-cycles consume low power by allocating different spectrum slots and modulation formats for each direction. A mixed integer linear programming (MILP) model is formulated to minimize total power consumption, which takes into account directed cycle generation, spectrum allocation, modulation adaptation, and protection capacity. To increase the scalability, the MILP model is decomposed, and a two-step approach is proposed: improved cycle enumeration and a simplified integer linear programming model. Extensive simulations are performed to study the power consumption of p-cycles under different traffic patterns in terms of traffic asymmetry ($TASY$), anycast ratio (AR), and the number of data centers (DCs). The results strongly demonstrate that directed p-cycles obtain significant power savings for protecting asymmetric traffic in EONs. The power savings rise up to 46.91% and 36.38% compared with undirected p-cycles as the $TASY$ and AR increase, respectively. Moreover, the directed p-cycles achieve valuable power savings (up to 46.1%) with the introduction of DCs while the amount of power savings does not depend on the number of DCs.**

***Index Terms*—Power savings, elastic optical networks (EONs), asymmetric traffic, pre-configured cycle (p-cycle).**

I. Introduction

ELASTIC optical networks (EONs) are the promising architectures to provision increasing traffic with flexible spectrum allocation and adaptive modulation formats [2]. Network survivability is increasingly important for EONs design against common network failures ($e.g.$, fiber cut) as growing number of services rely on the telecommunication infrastructure [3]. These growing traffic demands also consume increasing energy, which keeps an average annual growth rate of 10% in today's telecommunication networks since 2007 [4]. Survivable green EONs need to address both survivability and energy consumption [4]. However, most protection schemes for EONs only aimed at improving spectrum efficiency by solving the routing and spectrum allocation problem [3], [5]–[9]. Even though these protection schemes benefit from efficient spectrum allocation, they may consume more power due to the absence of power-aware optimization. In EONs, the power consumption of optical devices mainly comes from bandwidth variable transponders (BVTs), bandwidth variable cross-connects (BV-OXCs) and optical amplifiers (OAs) [10]. To meet the requirements on low power consumption, protection schemes for EONs need to take into account both power efficiency and spectrum efficiency.

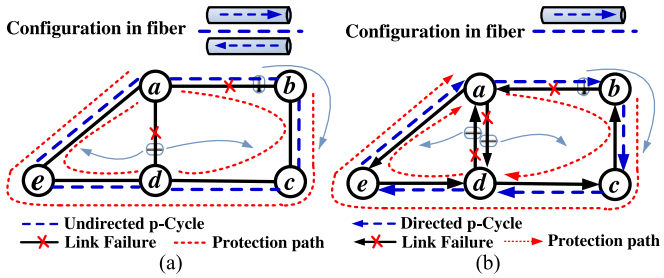

Fig. 1. Two kinds of p-cycles. (a) Undirected p-cycle protection (b) Directed p-cycle protection.

Moreover, EONs begin to support new networking capabilities and demanding network services. In addition to the conventional *symmetric traffic*, increasing new network services such as anycast service bring *asymmetric traffic* supported by data centers (DCs), $e.g.$, content delivery networks, distributed storage and virtual private networks [11]. Conventional symmetric traffic protection schemes assign the same amount of protection capacity in two directions between the same pair of nodes [12]. However, compared with the symmetric approach, it has been proved that asymmetric traffic provisioning can bring resource savings (up to 50% of spectrum usage and up to 30% of Capital Expenditure (CAPEX) cost) in EONs[11], thus protection schemes that focus on asymmetric traffic have big potential to achieve power savings.

Pre-configured Cycle (p-Cycle) protection scheme has attracted intense interest as it owns fast switching speed and provides protection capacity for both on-cycle links and straddling links [13]. There are two kinds of p-cycles, $i.e.$, undirected p-cycle and directed p-cycle, as shown in Fig. 1. Undirected p-cycle is the common protection strategy, in which the same protection capacity is configured in the two directions according to the maximum traffic amount of the two directional links.

Manuscript received April 28, 2016; revised June 30, 2016; accepted July 5, 2016. Date of publication July 11, 2016; date of current version August 12, 2016. This work was supported by China Scholarship Council Grant [2015]3022. A preliminary version of this work was presented as a postdeadline paper [1] at the European Conference on Network and Optical Communications Conference, June 2016, Lisbon, Portugal.

M. Ju is with the State Key Laboratory of Advanced Optical Communication Systems and Networks, Shanghai Jiao Tong University, Shanghai 200240, China, and also with the CERI-LIA (Computer Science Laboratory), University of Avignon, Avignon 84000, France (e-mail: min.ju@alumni.univ-avignon.fr).

F. Zhou is with the CERI-LIA (Computer Science Laboratory), University of Avignon, Avignon 84000, France (e-mail: fen.zhou@univ-avignon.fr).

S. Xiao is with the State Key Laboratory of Advanced Optical Communication Systems and Networks, Shanghai Jiao Tong University, Shanghai 200240, China (e-mail: slxiao@sjtu.edu.cn).

Z. Zhu is with the School of Information Science and Technology, University of Science and Technology of China, Hefei 230027, China (e-mail: zqzhu@ieee.org).

Color versions of one or more of the figures in this paper are available online at http://ieeexplore.ieee.org.

Digital Object Identifier 10.1109/JLT.2016.2590578

It means that once the undirected p-cycle is determined, the same spectrum slots and the same modulation format are configured in the two unidirectional fibers. Then, it enables to provide two units of protection capacity for each straddling link, as shown in Fig. 1(a) for $a-d$. However, directed p-cycle only configures protection capacity in one direction in the directed on-cycle links. Although a directed p-cycle provides one unit of protection capacity for each directed straddling link, $i.e.$, $a \rightarrow d$ and $d \rightarrow a$ in Fig. 1(b), it can distinguish directional links and provide different protection capacity for asymmetric traffic in two directions. Thus, the total protection capacity can be saved in directed p-cycles by efficiently allocating protection capacity for unidirectional link. Hence, directed p-cycles have the potential to protect the asymmetric traffic in a power-efficient way.

In our previous work, we studied undirected p-cycle design without candidate cycle enumeration in mixed line rates (MLR) networks [14]. Inspired by the advantage of $voltage$-based p-cycle generation and path-length-limited rate selection, we further explore directed p-cycle design for EONs and investigate the power savings of directed p-cycles for protecting asymmetric traffic. Specifically, a mixed integer linear programming (MILP) model called EDPC is formulated to minimize total power consumption in the considerations of directed cycle generation, spectrum allocation, modulation adaptation and protection capacity. Thereafter, to increase the scalability, EDPC is decomposed, and a two-step approach is proposed: improved cycle enumeration and a simplified integer linear programming (ILP) model called Decomposed EDPC (De-EDPC). We conduct extensive simulations to evaluate the power savings of proposed directed p-cycles compared with undirected p-cycle in terms of diverse traffic asymmetry ($TASY$), anycast ratio (AR) and the number of DCs. The key contributions of this paper are summarized as follows:

1) To the best of our knowledge, this is the first work on power-efficient protection for asymmetric traffic in EONs. Specifically, directed p-cycles are studied to earn power savings compared with traditional undirected p-cycles which are designed for symmetric traffic protection.
2) Directed p-cycles are explored in the considerations of cycle generation, spectrum allocation and adaptive modulation formats under transmission reach limits.
3) An MILP model is formulated to directly generate directed p-cycles without candidate cycle enumeration so that it is guaranteed to reach the optimal solution. To enable the scalability, a two-step approach is developed to solve the MILP model.
4) Extensive simulations are carried out to explore the power savings of directed p-cycles in terms of TASY, AR and the number of DCs in EONs. It is observed that directed p-cycles achieve power savings up to 47.9% compared with undirected p-cycles.

The rest of this paper is organized as follows. Related work is reviewed in Section II. Then, problem statement is addressed in Section III. The MILP formulation is developed in Section IV and the related two-step approach is proposed in Section V. Thereafter, simulation results are analyzed in Section VI. Finally, we conclude the paper in Section VII.

TABLE I
PROTECTION SCHEMES IN EONS

Objective	Symmetric traffic	Asymmetric traffic (including anycasting)
Spectrum-efficient	[5-9]	[18] ,[20]
Energy-efficient	[10],[15-17]	—

II. RELATED WORK

We summarize the existing protection schemes in EONs in terms of objective and traffic patterns in Table I. Most of these schemes focus on improving spectrum efficiency for either symmetric or asymmetric traffic protection, and energy-efficient protection schemes have been aroused to be investigated for symmetric traffic recently. However, there is no work on the energy-efficient protection scheme for asymmetric traffic in the consideration of new asymmetric services in EONs.

For the energy-efficient protection schemes, the authors in [4] addressed that energy efficiency and resilience needed to be combined in network design, and they also identified several challenges for energy-efficient survivable optical network design. In [15], the protection scheme under hourly traffic bandwidth requirement was studied in an energy-efficient way in single line rate, MLR and EON scenarios. In [16], the energy efficiency was evaluated in a differentiated quality of protection scheme by providing different protection levels for each connection, according to the client protection requirements. An energy-efficient hybrid path protection approach based on adaptive routing was studied with the introduction of regenerator activation in [17]. The authors in [10] discussed three power-aware protection schemes, referred to 1 + 1 dedicated protection (DP), 1:1 DP and shared protection, and evaluated the cost efficiency and energy efficiency improvement in EONs in comparison with wavelength division multiplexing (WDM) networks.

For the asymmetric traffic provisioning in EONs, the authors in [18] investigated both symmetric and asymmetric models for lightpath provisioning with dedicated path protection (DPP), and they concluded that asymmetric traffic protection acquired significant savings of BVT up to 25%. The similar conclusion was obtained in [11], in which the authors concluded that asymmetric traffic provisioning can bring significant resource savings compared with the symmetric approach (up to 50% spectrum usage savings and 30% CAPEX cost savings). Moreover, for the new anycast service, the authors in [19] proposed a novel tabu search (TS) approach to simultaneously covering unicast and anycast traffic routing in EONs. In [20], the joint optimization of anycast and unicast traffic with survivability consideration in EONs was studied with the DPP scheme.

These path protection schemes may suffer from long restoration time when a failure happens, as a cooperation among several nodes is required to notify the affected connection, please refer to [21]–[23] for an extensive review of restoration time. As opposed to path protection, p-cycle protection schemes benefit from ring-like recovery speed, in which only the ending nodes of the failed link do the switching operation [13], [22]. Moreover, it earns mesh-like capacity efficiency, as both

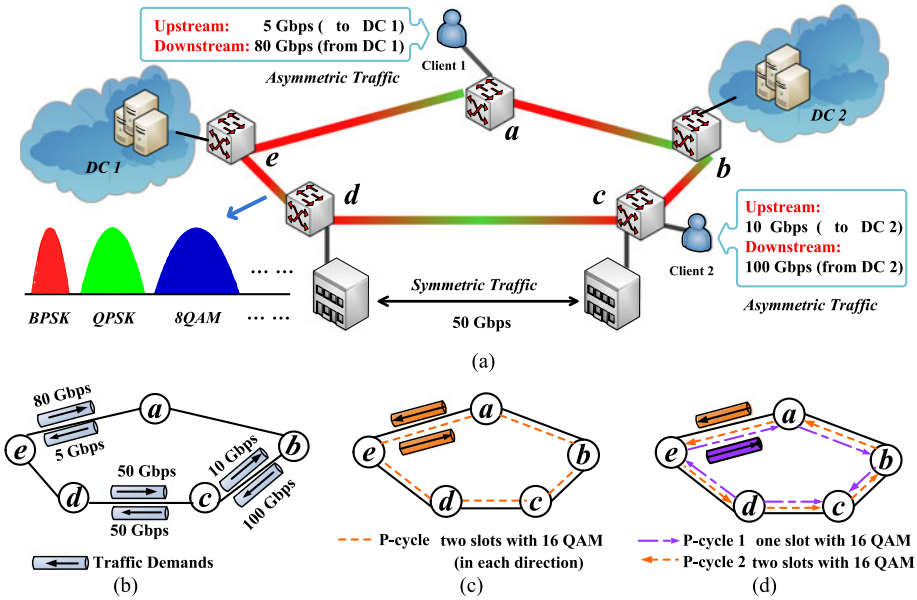

Fig. 2. (a) Symmetric and asymmetric services in EONs. (b) The traffic demands. (c) Undirected p-cycle protection. (d) Directed p-cycle protection.

on-cycle links and straddling links can be protected [13]. These benefits of p-cycle protection have driven several related investigations in WDM optical networks even though it has not been implemented in current optical networks. Recently, p-cycle protection scheme has been studied for EONs [5]–[7], [9]. The authors in [7] investigated dynamic p-cycle protection in EONs with spectrum planning related to protected working capacity envelope p-cycle design and Hamiltonian cycle. They further studied failure-independent path protection p-cycles taking into account routing, modulation formats and spectrum allocation in [5]. In [9], an ILP model for p-cycle design in EONs was developed to minimize total spectrum usage with load balancing in the working paths. An optimal design for p-cycle in EONs was studied with and without spectrum conversion in [6].

However, these p-cycle protection schemes only focused on minimizing spectrum usage without the consideration of power consumption. Meanwhile, most of the studied p-cycle designs were undirected p-cycles, which were not efficient for asymmetric traffic protection in EONs with new services. Directed p-cycle design has been carried out by Jaumard *et al.* in WDM networks [24], in which they concluded that using undirected p-cycles for asymmetric traffic protection required more resources than directed p-cycles (45% higher for pure asymmetric traffic). Nevertheless, their directed p-cycle scheme is no longer valid for EONs due to the absence of spectrum allocation and modulation format adaptation. Hence, power-efficient directed p-cycle design is urgent to be investigated for protecting asymmetric traffic in EONs.

III. Problem Statement

In EONs, asymmetric traffic between the clients and DCs become critical in addition to conventional symmetric traffic due to the new services such as anycast supported by DCs. Anycast service is defined as one to one-of-many transmission, in which client node v is fixed while the server node can be chosen among the set of admissible replica DCs [19]. Different from the conventional *symmetric traffic* which has the same traffic amount ($l^{Up} = l^{Down}$) in the upstream and downstream direction, *asymmetric traffic* differs in the two directions. More specifically, the upstream traffic l^{Up} is much smaller than the downstream traffic l^{Down}. We introduce a parameter called $TASY$ to describe the average $TASY$ in the network, given by Eq. (1). Specifically, for each pair of source node s and destination node d, l_{sd} and l_{ds} indicate the traffic demand in each direction, then the traffic asymmetry $TASY sd$ between s and d is calculated by Eq. (1) [24]. $TASY = 0\%$ represents symmetric traffic while $TASY = 100\%$ indicates pure asymmetric traffic.

$$TASY sd = \frac{max\{l_{sd}, l_{ds}\} - min\{l_{sd}, l_{ds}\}}{max\{l_{sd}, l_{ds}\} + min\{l_{sd}, l_{ds}\}} \times 100\% \quad (1)$$

$$TASY = \overline{TASY sd}.$$

For instance, Fig. 2(a) illustrates the symmetric and asymmetric services in EONs. The symmetric service consists of associated bidirectional symmetric traffic with the same volume in each direction, and asymmetric service with asymmetric traffic has different volumes in the upstream and downstream directions. Fig. 2(b) clearly illustrates the symmetric and asymmetric traffic. We assume EONs support contiguous frequency slices (FSs) with spectral width 12.5 GHz, which is also called *Spectrum Slot*. To protect the traffic with p-cycles, EONs support flexible FSs allocation and adaptive modulation formats (*i.e.*, BPSK, QPSK, 8 QAM and 16 QAM), which will be presented in the following part of power consumption. For simplicity, we assume that only 16 QAM with 50 Gbps protection capacity per slot is used in this example. Fig. 2(c) shows the conventional undirected p-cycle protection without consciousness of different traffic volumes in two directions, thus it assigns the same protection capacity (two FSs) in each direction to guarantee the protection. However, by distinguishing the different volume in each direction, directed p-cycle protection assigns

TABLE II
POWER CONSUMPTION OF A BVT WITH A SINGLE FS (12.5 GHZ) AT DIFFERENT MODULATION FORMATS[10]

Modulation Formats	TR (Gbps)	Power Consumption (W)
BPSK	12.5	112.374
QPSK	25	133.416
8QAM	37.5	154.457
16QAM	50	175.498

one FS for clockwise p-cycle 1 and two FSs for counterclockwise p-cycle 2, as shown in Fig. 2(d). It is obvious that directed p-cycle protection earns protection capacity savings in terms of FSs so that it is more suitable and valuable to investigate directed p-cycles to protect asymmetric traffic in EONs.

The extra protection capacity allocated for asymmetric traffic in undirected p-cycles also causes more power consumption because the optical devices such as BVTs, BV-OXCs, and OAs consume power depending on the number of occupied FSs and modulation formats. However, power consumption can be reduced by allocating different FSs and modulation formats in directed p-cycles according to the traffic volume in each direction. Thus, we investigate directed p-cycle protection for asymmetric traffic with the objective of minimizing power consumption against single link failure in EONs. The main considerations in this study are summarized as follows:

1) Power Consumption
   a) e_m^{BVT} *in* $\boldsymbol{BVT}$: The power consumption of BVT for a single FS e_m^{BVT} in Eq. (2) depends on the transmission rate (TR) in terms of modulation formats, as shown in Table II [10].

$$e_m^{BVT} = 1.683 \cdot TR + 91.333 \tag{2}$$

   b) e_v^{OXC} *in* BV-OXC: The power consumption of a BV-OXC e_v^{OXC} in Eq. (3) depends on its nodal degree D_v, the add/drop degree α and the additional contributions ($e.g.$, power supply, control cards) [10]. Here, we treat add/drop degree α as 9 at each node.

$$e_v^{OXC} = 85 \cdot D_v + 100 \cdot \alpha + 150. \tag{3}$$

   c) e_a^{EDFA} in OA: Erbium doped fiber amplifier (EDFA) is set as OA with span distance 80 km between two neighboring EDFAs. The number of EDFAs varies on each link depending on the link length d_a. We assume that an EDFA consumes 100 W per direction [10], [25]. Then, power consumption of EDFAs e_a^{EDFA} along link a is calculated in Eq. (4).

$$e_a^{EDFA} = \lfloor \frac{d_a}{80} + 1 \rfloor \cdot 100. \tag{4}$$

2) FSs Allocation
   a) *Spectrum continuity*: We assume that there is no spectrum conversion in the network. Thus, all the links in the same p-cycle should be assigned the same FSs.
   b) *Spectrum contiguousness*: We assume that the FSs allocated to the p-cycles are adjacent on the optical spectrum except the required guard band (GB). Note that in order to efficiently utilize the spectrum resources, the p-cycles can share the same FSs if they do not have any common link.
3) Modulation Format Adaptation
   a) *Protection capacity*: We consider the modulation format set M with BPSK, QPSK, 8-QAM and 16-QAM, then the protection capacity of one FS with each modulation format in M is 12.5, 25, 37.5 and 50 Gbps, respectively [10].
   b) *Transmission reach*: The corresponding maximum transmission reaches of these modulation formats are 9600, 4800, 2400 and 1200 km, respectively [26].

IV. MILP FORMULATION

In this section, we take into account all the considerations mentioned in Section III and develop an MILP model called EDPC to design power-efficient directed p-cycles for EONs. Inspired by the advantage of cycle generation method without candidate cycle enumeration in [14], we explore directed p-cycle generation so that the proposed EDPC model is guaranteed to reach the optimal solution. An EON can be modeled as a digraph $G(V, A)$, which has the OXCs set V and the directed links set A. Between two adjacent optical OXCs, there are two directed links, $e.g.$, link $v \rightarrow u$ denotes the directed link from node v to node u, which also can be represented by $a \in A$. The notations are in Table III. For the sake of readability, we use $\forall i$, $\forall v$, $\forall u$, $\forall m$, and $\forall a$ to denote $\forall i \in I$, $\forall v \in V$, $\forall u \in N_v$, $\forall m \in M$, and $\forall a \in A$, respectively.

A. Objective

$$\min \quad \gamma_1 \cdot (E_{BVTs} + E_{OXCs} + E_{EDFAs}) + \theta_1 \cdot t_b \tag{5}$$

The objective is to minimize the total power consumption of directed p-cycles and the maximum index of FSs usage t_b. The optimization of t_b guarantees the *spectrum contiguousness* and potential spectrum sharing among p-cycles. γ_1 and θ_1 are adjustable parameters for weighting of these two metrics.

The total network power consumption is composed of:

1) E_{BVTs}: The power consumption of BVTs

$$E_{BVTs} = \sum_{i \in I} \sum_{m \in M} \sum_{a \in A} 2 \cdot e_m^{BVT} \cdot \pi_a^{im}. \tag{6}$$

   E_{BVTs} is introduced at the starting node and ending node of the protection path. It is the product of the number of occupied FSs and the power consumption of a single FS corresponding to the modulation format in Table II.
2) E_{OXCs}: The power consumption of OXCs

$$E_{OXCs} = \sum_{i \in I} \sum_{v \in V} \sum_{u \in N_v} \frac{n_{vu}^i}{B} \cdot e_v^{OXC}. \tag{7}$$

TABLE III

Network Sets and Parameters	
I	The p-cycle set with maximum number $\|I\|$ allowed in EDPC, I_i indicates i-th p-cycle in I.
$G(V, A)$	Network topology with node set V and link set A.
N_v	The set of adjacent nodes of a node v.
M	The available modulation level set, $i.e.$, BPSK, QPSK, 8-QAM and 16-QAM.
d_{vu}	The length between node v and node u in $G(V, A)$, and L_{max} indicates the biggest length.
TR_m	The available bandwidth provided by one slot at modulation level m, which is $12.5, 25, 37.5$ and 50 Gbps for BPSK, QPSK, 8-QAM and 16-QAM, respectively.
e_m^{BVT}	The power consumption of the BVT at modulation m.
e_v^{OXC}	The power consumption of the BV-OXC at node v.
e_a^{EDFA}	The power consumption of all the EDFAs on link a.
h_m	Maximum transmission reach at modulation level m, which is 9600, 4800, 2400 and 1200 km for BPSK, QPSK, 8-QAM and 16-QAM, respectively [5]. h_{max}=9600 km, and h_{min}=1200 km.
N_G	The GB with one FS.
B	The available FSs on each fiber link, which is 320.
l_{vu}	Traffic load on unidirectional link $v \rightarrow u$ after routing.
β	A pre-defined fractional constant, $\frac{1}{\|V\|} \geq \beta > 0$.
Variables in EDPC	
$x_{vu}^i \in \{0, 1\}$	Equals 1 if link $v \rightarrow u$ is used by I_i, and 0 otherwise.
$y_v^i \in \{0, 1\}$	Equals 1 if node v is crossed by I_i, and 0 otherwise.
$f_v^i \in \{0, 1\}$	Virtual $voltage$ value of node v in I_i.
$o_v^i \in \{0, 1\}$	Equals 1 if node v is root node in I_i, and 0 otherwise.
$b_m^i \in \{0, 1\}$	Equals 1 if I_i operates at modulation level m, and 0 otherwise.
$q_{vu}^i \in \{0, 1\}$	Equals 1 if link $v \rightarrow u$ desires to be protected by I_i, and 0 otherwise.
$c_{ij} \in \{0, 1\}$	Equals 1 if I_i and I_j have at least one common link, and 0 otherwise.
$s_i \in [0, B]$	The starting index of FSs in I_i.
$o_{ij} \in \{0, 1\}$	Equals 1 if the starting index of FSs in I_i is smaller than that in I_j, and 0 otherwise.
$n_i \in [0, 32]$	The number of occupied FSs of I_i. The maximum FSs is 32 due to the capacity limitation in BVT.
$t_b \in [0, B]$	The maximum index of occupied FSs in all the p-cycles.
$\pi_{vu}^{im} \in [0, 32]$	The number of FSs provided by I_i to protect link $v \rightarrow u$ at modulation level m.
$n_{vu}^i \in [0, 32]$	The number of occupied FSs of I_i on link $v \rightarrow u$.

E_{OXCs} is calculated based on the proportion of resources that the protection path occupies in the links (number of occupied FSs with respect to the total FSs in a fiber).

3) E_{EDFAs}: The power consumption of EDFAs

$$E_{EDFAs} = \sum_{i \in I} \sum_{a \in A} \frac{n_a^i}{B} \cdot e_a^{EDFA}. \tag{8}$$

E_{EDFAs} is calculated in the same way as E_{OXCs}.

B. Constraints

The constraints in EDPC can be classified into **Directed cycle generation constraints** (9)-(13), **FSs allocation constraints** (18)-(22), **modulation adaptation constraints** (23)-(24) and **protection capacity constraints** (25)-(29).

1) Directed Cycle Generation Constraints: Constraint (9) ensures that at most one unidirectional link between two nodes can be used in a directed p-cycle. Constraints (10) and (11) ensure that if node v is crossed by a p-cycle, then it must own one incoming link and one outgoing link. In order to guarantee that only a single cycle is generated, we further formulate constraints (12) and (13) to eliminate other cycles with $voltage$ conflict and make sure the generated cycle is a connected graph, as shown in Fig. 3. These constraints enable to generate single directed p-cycle with either clockwise or counterclockwise. We prove it in Theorem 1.

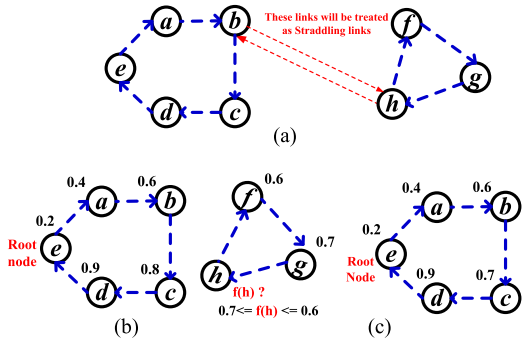

Fig. 3. Single directed cycle generation with $voltage$ and $root$. (a) Invalid Two cycles for one directed p-cycle without "voltage". b) Voltage conflict. (c) Valid p-cycle generation with "voltage."

$$x_{vu}^i + x_{uv}^i \leq 1, \qquad \forall i, \forall v, \forall u \tag{9}$$

$$\sum_{u \in N_v} x_{uv}^i - \sum_{u \in N_v} x_{vu}^i = 0, \qquad \forall i, \forall v \tag{10}$$

$$y_v^i = \sum_{u \in N_v} x_{vu}^i, \qquad \forall i, \forall v \tag{11}$$

$$f_u^i - f_v^i + o_u^i \geq (1 + \beta) \cdot x_{vu}^i - 1, \qquad \forall i, \forall v, \forall u \tag{12}$$

$$\sum_{v \in V} o_v^i \leq 1, \qquad \forall i. \tag{13}$$

Theorem 1: Constraints (9)-(13) guarantee to generate a single directed p-cycle with either clockwise or counterclockwise for each $i \in I$.

Proof: According to constraints (9)-(11), for each $i \in I$, each node in I_i either has both an incoming link and an outgoing link, or does not have any adjacent link. Thus, a single directed cycle or several ones are generated for I_i (clockwise or counterclockwise). In the latter case, several directed cycles can not be used as one directed p-cycle. As we can see from Fig. 3(a), if these two cycles are regarded as one p-cycle I_i, the links $b \rightarrow h$ and $h \rightarrow b$ would have the potential to be protected by I_i because nodes b and h are crossed by I_i. Obviously, this is not correct.

Next, we prove by contradiction that only a single cycle is permitted with the help of constraints (12) and (13). Without loss of generality, we suppose that two directed cycles are generated by constraints (9)-(11) in Fig. 3(b), and node e is the only $root\ node$, where the value beside each node indicates the corresponding voltage value. We can find that the cycle consisting of nodes f, g, h can not exist due a voltage conflict explained as follows. Since there is no root node, $i.e.$, $o_f^i = 0$, $o_h^i = 0$ and $o_g^i = 0$, we can get the following inequalities by using

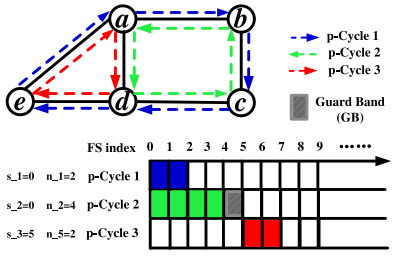

Fig. 4. FSs allocation for different directed p-cycles.

constraint (12),

$$f_f^i - f_h^i \geq \beta \tag{14}$$

$$f_g^i - f_f^i \geq \beta \tag{15}$$

$$f_h^i - f_g^i \geq \beta. \tag{16}$$

Adding the three inequalities, a voltage conflict occurs: $0 \geq \beta$.

However, constraints (12) and (13) permit to generate a single cycle ($e.g.$, the cycle consisting of nodes a, b, c, d, e) with the root node in Fig. 3(c). From constraint (12), we can see that for each directed link, ending node has a bigger voltage than the staring node except the link $d \rightarrow e$ with ending root node e. However, by assigning $o_e^i = 1$ to the root node, the previous voltage conflict problem can be avoided. Thus, constraint (12) can be rewritten as

$$f_e^i - f_d^i + 1 \geq \beta. \tag{17}$$

Hence, root node e is able to have a smaller voltage than node d. Furthermore, the voltage conflict $0 \geq \beta$ can thus be avoided, since we will get $1 \geq \beta$ instead by adding all the inequalities. Thus, the proof follows.

2) FSs Allocation Constraints: Constraints (18)-(20) allocate the order of FSs for each p-cycle. Constraint (18) indicates whether two p-cycles have any common link. Constraint (19) makes the comparison of starting index of FSs between two p-cycles. Constraint (20) avoids spectrum conflict by adding GB and also ensures that two p-cycles can share the same FSs if they do not have any common link. Constraint (21) implies the maximum index of FSs, which is minimized in Eq. (5) to ensure *spectrum contiguousness*. Constraint (22) indicates the *spectrum continuity* along the links in one p-cycle.

$$x_a^i + x_a^j - 1 \leq c_{ij}, \qquad \forall i, j, i \neq j, \forall a \tag{18}$$

$$o_{ij} + o_{ji} = 1, \qquad \forall i, j, i \neq j \tag{19}$$

$$s_i + n_i + N_G - s_j \leq B \cdot (2 - o_{ij} - c_{ij}), \qquad \forall i, j, i \neq j \tag{20}$$

$$s_i + n_i \leq t_b, \qquad \forall i \tag{21}$$

$$n_a^i = x_a^i \cdot n_i, \qquad \forall i, \forall a. \tag{22}$$

An example of FSs allocation for three p-cycles is shown in Fig. 4. In each p-cycle, the same FSs are used on all the links. In addition, p-cycle 1 and p-cycle 2 can share some FSs with index 1 and 2 as they do not have any common link. However, for p-cycle 2 and p-cycle 3 with the common link $a \rightarrow d$, GB with index 5 should be reserved between the occupied FSs.

3) Modulation Adaptation Constraints: Constraint (23) guarantees modulation format selection with maximum transmission reach consideration. Constraint (24) ensures that only one modulation format can be assigned for one p-cycle.

$$\frac{\sum_{a \in A} d_a \cdot x_a^i - q_a^i \cdot d_a}{h_m} \leq \frac{h_{max}}{h_{min}} \cdot (1 - b_m^i) + \frac{L_{max}}{h_m} \cdot (1 - q_a^i) + b_m^i, \qquad \forall i, \forall m, \forall a \tag{23}$$

$$\sum_{m \in M} b_m^i \leq 1, \qquad \forall i. \tag{24}$$

Note that the modulation format of a p-cycle is selected depending on the length of each protection path instead of the circumference of p-cycle so that more flexible modulation format can be assigned to ensure power-efficient p-cycle design. For instance, a p-cycle whose circumference exceeds 1200 km still can be assigned with 16-QAM if all of its protection paths are shorter than 1200 km. This is called path-length-limited p-cycle, which has the advantage over cycle-circumference-limited p-cycle as studied in [14], [27].

4) Protection Capacity Constraints: Constraints (25) and (26) indicate the desire of link $v \rightarrow u$ to be protected by I_i, providing that its two ending nodes v and u are crossed by I_i, and it is not an on-cycle link. Note that both the on-cycle links and straddling links are guaranteed to be protected only when they desire to be protected. Constraint (27) indicates the protection capacity of FSs that provided by I_i at modulation level m to protect link a. Constraint (28) ensures the maximum capacity of a BVT is 400 Gbps [10]. Constraint (29) ensures 100% single link failure protection.

$$q_{vu}^i \leq \frac{1}{2}(y_v^i + y_u^i), \qquad \forall i, \forall v, \forall u \tag{25}$$

$$q_a^i \leq 1 - x_a^i, \qquad \forall i, \forall a \tag{26}$$

$$\pi_a^{im} \leq q_a^i \cdot b_m^i \cdot n_i, \qquad \forall i, \forall m, \forall a \tag{27}$$

$$\pi_a^{im} \cdot TR_m \leq 400, \qquad \forall i, \forall m, \forall a \tag{28}$$

$$\sum_{i \in I} \sum_{m \in M} \pi_a^{im} \cdot TR_m \geq l_a, \qquad \forall a. \tag{29}$$

In order to ensure linearity, constraints (22) and (27) are rewritten as constraints (30) and (31), respectively.

$$\Longrightarrow \begin{cases} n_a^i \leq n_i, & \forall i, \forall a \\ n_a^i \leq x_a^i \cdot 32, & \forall i, \forall a \\ n_a^i \geq n_i - (1 - x_a^i) \cdot 32, & \forall i, \forall a \end{cases} \tag{30}$$

$$\Longrightarrow \begin{cases} \pi_a^{im} \leq n_i, & \forall i, \forall m, \forall a \\ \pi_a^{im} \leq q_a^i \cdot 32, & \forall i, \forall m, \forall a \\ \pi_a^{im} \leq b_m^i \cdot 32, & \forall i, \forall m, \forall a. \end{cases} \tag{31}$$

Note that $|I|$ (the maximum number of p-cycle allowed in EDPC) is a predetermined parameter. It should be sufficiently large to ensure that the proposed EDPC manages to obtain the optimal solution. However, a larger $|I|$ will slow down the

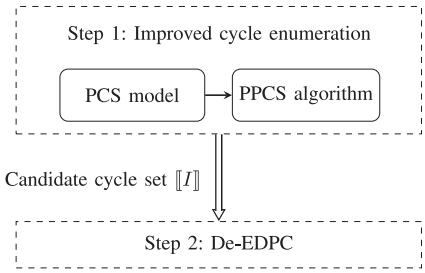

Fig. 5. Flow chart for the two-step approach.

execution time because for a given network the number of variables and constraints increases largely with $|I|$. For solving the EDPC, we set the number of p-cycles $|I|$ based on the protection capacity limitation in BVT. For each $a \in A$, we choose the possible number of p-cycles (with 400 Gbps) to protect it. Then, the total number of p-cycles $|I|$ can be estimated by Eq. (32) considering that a p-cycle can protect at least 3 links. In addition, a small positive integer δ is added in case that $|I|$ is not large enough.

$$|I| = \delta + \frac{1}{3}\sum_{a\in A}\lceil\frac{l_a}{400}\rceil. \tag{32}$$

C. Discussion

In the proposed EDPC, directed p-cycles are designed with the objective of minimizing the total power consumption. As the power optimization has the priority over the spectrum optimization, it may occur that more FSs are utilized in order to satisfy lower power consumption. Thus, there is a tradeoff between power and spectrum optimization when designing the p-cycle protection scheme for EONs. The model can be extended to represent the conventional p-cycle design without power consideration for asymmetric traffic protection by redefining the objective function of power consumption to total spectrum usage as follows:

$$\min \quad \gamma_2 \cdot S_{Total} + \theta_2 \cdot t_b \tag{33}$$

$$S_{Total} = \sum_{i\in I}\sum_{a\in A} n_a^i. \tag{34}$$

Here, γ_2 and θ_2 are two adjustable parameters for the weights of total FSs allocated for protection capacity and the maximum index of the occupied FSs.

V. A Two-Step Approach

Owing to the absence of candidate cycle enumeration, EDPC can reach the optimal solution, but its high computational complexity causes the scalability problem. It is why we decompose it into a two-step approach: improved cycle enumeration and a simplified ILP model called De-EDPC. As shown in the flow chart in Fig. 5, improved cycle enumeration is implemented by a promising power-efficient p-cycles selection (PPCS) algorithm to pre-compute the candidate cycle set for De-EDPC, while the latter is a simplified formulation decomposed from EDPC.

Algorithm 1: PPCS Algorithm

Input : $G(V, A)$, h_m, $\forall m \in M$, $m = 0,1,2,3$.
Output: Selected candidate cycle set $[\![I]\!]$

```
for m ∈ M do
    if m < 3 then
        enumerate the complete cycle set [[Î]] whose
        circumference in the range (h_{m+1}, h_m] using the
        approach in [28];
    else
        enumerate the complete cycle set [[Î]] whose
        circumferences in the range (0, h_3] using the
        approach in [28];
    solve the PCS model with the complete cycle set [[Î]];
    store the selected cycles obtained from PCS model in
    [[I]];
output [[I]]
```

TABLE IV

Network Sets and Parameters in PCS	
$[\![\hat{I}]\!]$	Complete candidate cycle set obtained by the method in [28].
$x_a^i \in \{0,1\}$	Equals 1 if cycle $\hat{I}_i$ crosses link a, and 0 otherwise.
$z_a^i \in \{0,1\}$	Equals 1 if cycle $\hat{I}_i$ can protect link a, and 0 otherwise.
Variables in PCS	
$w_i \in \{0,1\}$	Equals 1 if cycle $\hat{I}_i$ is selected from $[\![\hat{I}]\!]$, and 0 otherwise.

A. Improved Cycle Enumeration

The main idea of the improved cycle enumeration is that we select just enough p-cycles with different circumferences corresponding to maximum transmission reach limits so that the selected p-cycles for De-EDPC can be assigned diverse modulation formats power-efficiently. Thus, PPCS algorithm is developed to pre-compute the candidate cycle set and reduce the computation complexity for De-EDPC model, which will be explained in detail in Section V-B. However, the method in [28] enumerates a large complete set $[\![\hat{I}]\!]$ of p-cycles, which results in high computation complexity. So we develop the following p-cycle selection (PCS) ILP model to select just enough p-cycles from $[\![\hat{I}]\!]$. The parameters and variables are shown in Table IV. The objective of PCS is to minimize the total number of links in all the selected p-cycles. Constraint (36) ensures that the selected p-cycles should be able to protect all the links that can be initially protected by p-cycles in the complete candidate cycle set $[\![\hat{I}]\!]$.

$$min \sum_{i\in[\![\hat{I}]\!]}\sum_{a\in A} w_i \cdot x_a^i \tag{35}$$

$$\sum_{i\in[\![\hat{I}]\!]} w_i \cdot z_a^i \geq z_a^i, \forall i, \forall a. \tag{36}$$

TABLE V

New Network Sets and Parameters in De-EDPC	
$[\![I]\!]$	Selected candidate cycle set obtained by PPCS algorithm.
$x_a^i \in \{0,1\}$	Equals 1 if cycle I_i crosses link a, and 0 otherwise.
$z_a^i \in \{0,1\}$	Equals 1 if cycle I_i can protect link a, and 0 otherwise.
$c_{ij} \in \{0,1\}$	Equals 1 if cycle I_i and I_j have at least one common link, and 0 otherwise.
Variables in De-EDPC	
$b_m^i \in \{0,1\}$	Equals 1 if I_i operates at modulation level m, and 0 otherwise.
$q_{vu}^i \in \{0,1\}$	Equals 1 if link $v \to u$ desires to be protected by I_i, and 0 otherwise.
$s_i \in [0,B]$	The starting index of FSs in I_i.
$o_{ij} \in \{0,1\}$	Equals 1 if the starting index of FSs in I_i is smaller than that in I_j, and 0 otherwise.
$n_i \in [0,32]$	The number of occupied FSs of I_i. The maximum FSs is 32 due to the capacity limitation in BVT.
$t_b \in [0,B]$	The maximum index of occupied FSs in all the p-cycles.
$\pi_{vu}^{im} \in [0,32]$	The number of FSs provided by I_i to protect link $v \to u$ at modulation level m.

$Algorithm$ 1 shows the PPCS procedure. Considering the different maximum transmission reaches of modulation format set M, $Lines$ 2-5 explain how to enumerate the complete cycle set with different circumferences. $Line$ 6 performs PCS model to select just enough cycles from the enumerated cycles. We store the selected cycles in $[\![I]\!]$. Thus, we obtain the candidate cycles with different circumferences for De-EDPC.

For the PPCS algorithm, we only use it once to obtain the candidate cycle set in the network initialization. Thus, it will not cause intolerable computational complexity afterwards.

B. Decomposed EDPC

As De-EDPC is decomposed from EDPC in Section IV, the similar variables and constraints are used. We summarize the parameters and variables of De-EDPC in Table V. Note that instead of using a specific cycle repeat variable, we use an equivalent method that scales the candidate cycle set $[\![I]\!]$ by repeating the cycles several times according to the total traffic volume. Thus, the parameters x_a^i, z_a^i and c_{ij} can be determined in advance. There are some changes in the objective functions Eqs. (7) and (8) as follows,

$$E_{OXC} = \sum_{i \in [\![I]\!]} \sum_{v \in V} \sum_{u \in N_v} \frac{x_{vu}^i \cdot n_i}{B} \cdot e_v^{OXC} \tag{37}$$

$$E_{EDFA} = \sum_{i \in [\![I]\!]} \sum_{a \in A} \frac{x_a^i \cdot n_i}{B} \cdot e_a^{EDFA}. \tag{38}$$

The majority constraints in De-EDPC are the same as in EDPC, including **FSs allocation** (19)-(21), **Modulation adaptation** (23)-(24), **Protection capacity** (27)-(29). However, constraints (25) and (26) are replaced by constraint (39).

$$q_a^i \le z_a^i, \qquad \forall i, \forall a \tag{39}$$

TABLE VI
COMPUTATIONAL COMPLEXITIES OF EDPC AND DE-EDPC

Models	Computational complexities	
	No. of Dominant Variables	No. of Dominant Constraints
EDPC	$max\{O(\|I\|\|A\|), O(\|I\|^2)\}$	$O(\|I\|^2\|A\|)$
De-EDPC	$max\{O(\|[\![I]\!]\|\|A\|), O(\|[\![I]\!]\|^2)\}$	$max\{O(\|[\![I]\!]\|\|A\|), O(\|[\![I]\!]\|^2)\}$

C. Computational Complexity

The number of dominant variables and constraints in EDPC and De-EDPC is summarized in Table VI (we assign $|M| = 4$ as we have four modulation formats). The number of dominant variables is the same in these two models while the number of dominant constraints in De-EDPC is largely reduced. The computational complexities in terms of dominant variables and constraints are still big for large-size networks, efficient heuristic algorithms will be developed as our future work. However, in this work, we mainly focus on studying the advantages of directed p-cycles for asymmetric traffic protection in EONs by developing ILP models.

VI. PERFORMANCE EVALUATIONS

We use CPLEX 12.06 to solve the proposed De-EDPC on an Intel Core PC equipped with a 3.5 GHz CPU and 8 GBytes RAM. The following test beds are used: NSFNET (**14 nodes**, **44 directed links** and **average nodal degree 3.1**) in Fig. 6(b) [29] and US Backbone networks (**28 nodes**, **90 directed links** and **average nodal degree 3.2**) in Fig. 6(c) [29]. We regard γ_1 and θ_1 as 1 in the objective function Eq. (5) as it helps to improve the optimization speed for a high quality solution. Note that it has little impact on the first priority of total power consumption in our study. First, we evaluate the quality of solution in De-EDPC compared with the solution in EDPC. Then, extensive simulations are performed to show the power savings in De-EDPC in terms of TASY, AR and the number of DCs. AR is defined as the proportion of anycast traffic in the total traffic in the network. The following three metrics are used to evaluate the performance of p-cycles:

1) $Power\ Consumption$: Our goal is to minimize the power consumption of p-cycles for asymmetric traffic protection.
2) $Power\ Savings\ in$ *De-EDPC*: This metric shows the advantage of power savings through power-efficient directed p-cycles in proposed De-EDPC.
3) $Total\ FS\ Usage$: Total FS usage is an important feature that indicates the spare capacity usage of p-cycles.

A. Quality of Solution in De-EDPC

To verify the efficiency of the solutions in De-EDPC, we perform both EDPC and De-EDPC in six-node and NSFNET networks with small traffic demands. A server with 500 GBytes memory is used due to the high computation complexity in EDPC while De-EDPC is solved in a PC with 8 GBytes memory. The traffic is generated with $TASY = 20\%$ and set up by

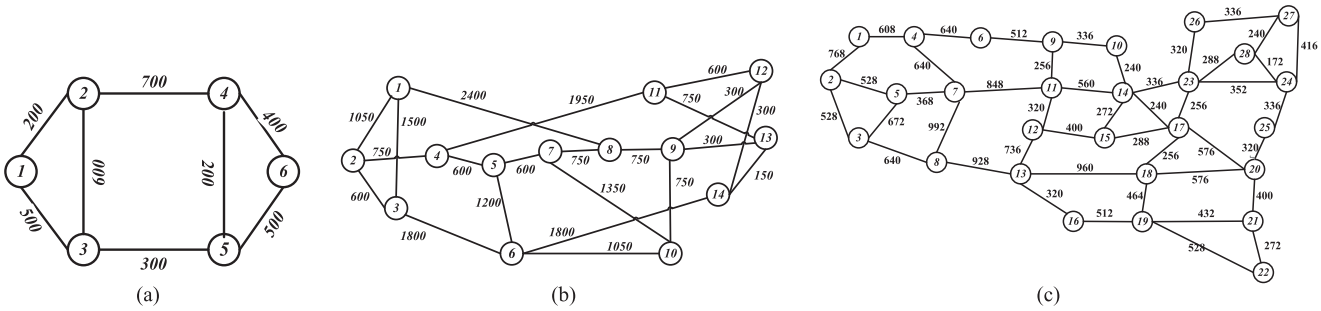

Fig. 6. The network typologies used in the simulations. (a) The six-node network topology [5]. (b) The NSF network topology [29]. (c) The US Backbone network topology [29].

TABLE VII
QUALITY OF SOLUTION AND EXECUTION TIME IN EDPC AND DE-EDPC

Six-node network						NSFNET network					
Traffic	EDPC ($\|I\|=6$)		De-EDPC ($\|[\![I]\!]\|=6$)		Gap	Traffic	EDPC ($\|I\|=15$)		De-EDPC ($\|[\![I]\!]\|=20$)		Gap
	Results	Execution Time	Results	Execution Time			Results	Execution Time	Results	Execution Time	
$1X$	4521.69	3146.89 s	4712.23	0.18 s	4.04%	$1X$	10260.7	21270.66 s	10299.9	0.39 s	0.38%
$2X$	6357.91	2818.22 s	7018.97	0.52 s	9.42%	$2X$	11084.6	26547.16 s	11997.4	0.57 s	7.61%

* The basic traffic 1X is 320 Gbps and 100 Gbps in six-node and NSFNET networks, respectively.

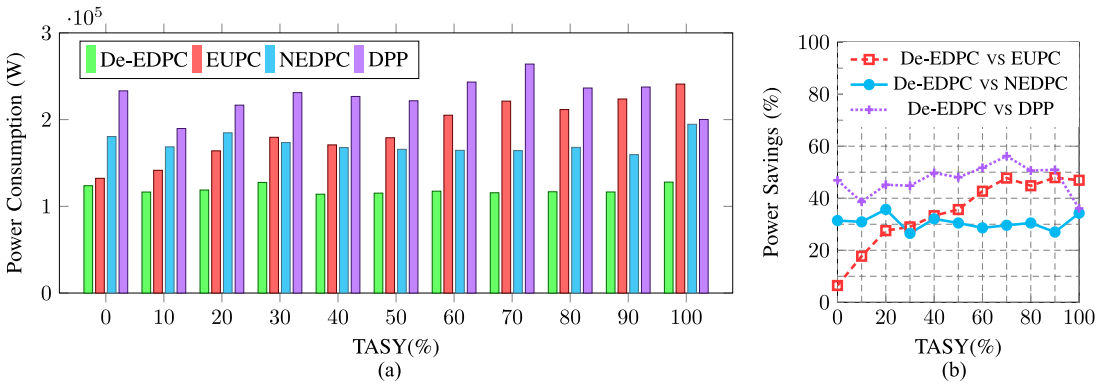

Fig. 7. Power consumption as a function of TASY in NSFNET network. (a) Power consumption. (b) Power savings in De-EDPC.

Dijkstra's shorted-path routing. By using Eq. (32), we set the number of allowed cycles in EDPC as $|I| = 6$ and $|I| = 15$ in six-node and NSFNET networks, respectively. The number of candidate cycles in De-EDPC is obtained by PPCS algorithm with $[\![I]\!] = 6$ and $[\![I]\!] = 20$ in six-node and NSFNET networks, respectively.

Table VII shows the results. Only a small traffic is shown because the EDPC exceeds the memory for a higher traffic. As we can see that De-EDPC achieves comparable solutions and dramatically reduces execution time compared with EDPC especially for a larger topology. For instance in NSFNET network, it requires more than 7 h to obtain the solution in EDPC while it takes less than 1 s in De-EDPC. The large reduction of execution time in De-EDPC is very attractive even though a small optimality gap is introduced. The optimality gap is because De-EDPC has relatively smaller feasible region compared with EDPC due to the fixed candidate cycles.

We can conclude that the proposed PPCS algorithm and De-EDPC offers a time-efficient way to solve the directed p-cycle design problem with high quality solutions.

B. Impact of $TASY$ on Power Savings in De-EDPC

We then study the power consumption of p-cycles for asymmetric traffic protection with De-EDPC in NSFNET and US Backbone networks. The traffic is generated with $TASY \in [0\%, 100\%]$. To evaluate the power savings of power-efficient directed p-cycles in De-EDPC, the following benchmarks are used:

1) EUPC: It develops undirected p-cycles that minimize the total power consumption. We formulate the ILP model for EUPC based on De-EDPC. Note that EUPC enables the twice protection capacity for each straddling link.
2) NEDPC: It is modified from the optimal p-cycle design in [6], which is formulated to minimize the sum of total FSs

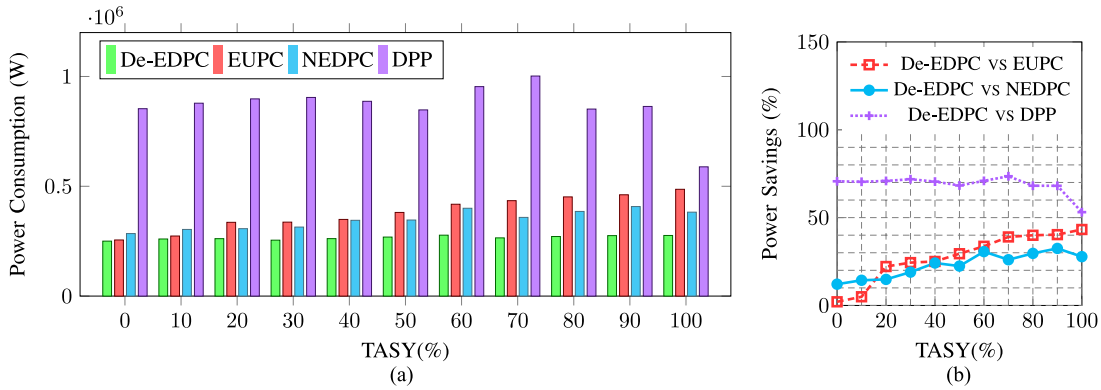

Fig. 8. Power consumption as a function of TASY in US Backbone network. (a) Power consumption. (b) Power savings in De-EDPC.

usage and maximum index of FSs. We add modulation formats and transmission reach limits in NEDPC to make a fair comparison.

3) DPP: It is the DPP that we adapt from DP 1+1 protection in [10] by adding the same physical conditions as in De-EDPC. According to the working path calculated in advance, we compute *K* link-disjoint paths as candidate backup paths.

The total power consumption of all the potential single link failures in De-EDPC, EUPC, NEDPC and DPP are shown in Figs. 7 and 8 for NSFNET and US Backbone networks, respectively. As we can observe that DPP consumes more power than these p-cycle schemes, especially compared with the proposed De-EDPC. This is because that all the demands affected by the failed link in DPP need to be rerouted from the corresponding source nodes to the destination nodes while p-cycle protection schemes only reroute the traffic on the failed link between the two adjacent nodes. Thus, the more protection paths with bigger distance in DPP consume more power than the p-cycle protection. Among these three p-cycle schemes, De-EDPC consumes the lowest power for all of $TASY$, and the amount of power consumption in De-EDPC maintains the same level. As $TASY$ increases, the power consumption in EUPC goes up and it becomes the biggest. The power consumption in NEDPC also does not change too much with the increase of $TASY$. From Figs. 7(b) and 8(b), it is observed that the average power savings in De-EDPC compared with DPP is even 47.1% in NSFNET and 68.8% in US Backbone. For these p-cycle schemes, the power savings in De-EDPC compared with EUPC grow with the increase of $TASY$ from 0% to 100% ($i.e.$, from symmetric traffic to pure asymmetric traffic). For $TASY = 0\%$, the power saving is 6.46% in NSFNET network and 2.08% in US Backbone network. For $TASY = 100\%$, the power saving is even 46.91% in NSFNET network and 43.24% in US Backbone network. However, the power savings in De-EDPC compared with NEDPC does not show the same trend in NSFNET and US Backbone networks. It maintains among $(26\%, 36\%)$ in NSFNET network, but it grows a little (from 12% to 33%) with increase of $TASY$ in US Backbone network.

We also study the total number of used cycles and FSs usage in De-EDPC, EUPC, and NEDPC to make a fair comparison in Table VIII. We can see that as $TASY$ increases, the total number of used p-cycles does not show many differences in De-EDPC, EUPC and NEDPC, respectively. However, the total number of FSs usage grows a lot with the increase of $TASY$ in these three p-cycle schemes. Among them, it is observed that NEDPC requires fewer p-cycles and FSs compared with De-EDPC and EUPC. This is because it is optimized to minimize spectrum usage, then high spectrum efficiency leads to fewer p-cycles. De-EDPC outperforms EUPC in terms of FSs usage because EUPC allocates twice the number of FSs for the undirected p-cycles without consciousness of the different traffic volume while De-EDPC effectively allocates the FSs according to the different traffic volume in each direction.

The simulation results demonstrate that directed p-cycles in De-EDPC provide a power-efficient way to protect asymmetric traffic in EONs. p-Cycle protection schemes consume less total power of all the potential link failures than the DPP scheme. De-EDPC earns significant power savings (up to 46.91%) against undirected p-cycles in EUPC, especially for asymmetric traffic with high $TASY$. De-EDPC also requires fewer FSs than EUPC. De-EDPC owns power consumption advantage over NEDPC, but it requires more FSs.

C. Impact of AR on Power Savings in De-EDPC

We then study the power savings in De-EDPC when both anycast and unicast services are considered. Specifically, the total traffic is composed of unicast traffic that generated between a pair of nodes, and anycast traffic that generated between the clients and DCs. We assume three DCs are located at nodes 1, 8 and 14 in NSFNET network, and six DCs are located at nodes 1, 7, 14, 19, 21 and 28 in US Backbone network. We use AR that corresponds to 0%, 20%, 40%, 60% and 80%. The total traffic is 4 Tbps and 8 Tbps in NSFNET and US Backbone networks, respectively.

Fig. 9(a) and (b) illustrate the total power consumption of the three p-cycle schemes and power savings in De-EDPC in NSFNET and US Backbone networks, respectively. For the total power consumption, as the AR increases, De-EDPC consumes the relatively stable power amount while EUPC requires more power in both NSFNET and US Backbone networks. We can see that the power savings in De-EDPC compared with EUPC increases from 6.46% (at $AR = 0\%$) to 36.38% (at $AR = 80\%$)

TABLE VIII
TOTAL NUMBER OF p-CYCLES AND FSS IN NSFNET AND US BACKBONE NETWORKS

TASY	NSFNET						US Backbone					
	De-EDPC		EUPC		NEDPC		De-EDPC		EUPC		NEDPC	
	Cycles	FSs	Cycles	FSs	Cycles	FSs	Cycles	FSs	Cycles	FSs	Cycles	FSs
0%	37	1385	36	1546	18	969	55	1635	50	1748	38	1349
20%	43	1247	38	2036	17	867	53	1834	54	2220	39	1563
40%	40	1194	46	2088	19	860	56	1903	56	2306	37	1603
60%	41	1334	42	2246	18	1018	58	2805	50	2788	39	2251
80%	40	1391	40	2546	20	1062	59	3057	56	3138	38	2483
100%	39	2007	40	3216	13	1482	58	3292	62	3278	40	2548

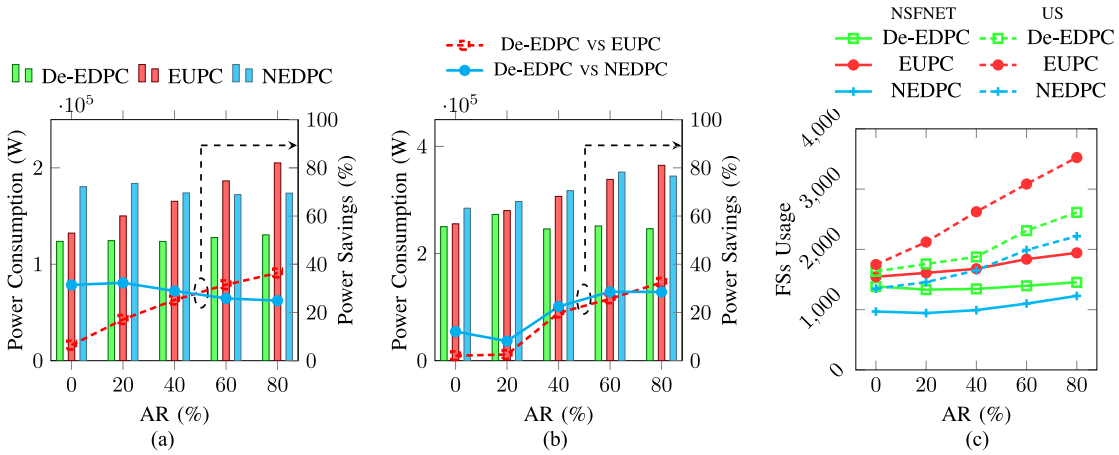

Fig. 9. Power consumption and total FSs usage as a function of AR. (a) Power consumption and power savings in De-EDPC in NSFNET network. (b) Power consumption and power savings in De-EDPC in US Backbone network. (c) Total FSs usage in NSFNET and US Backbone networks.

in NSFNET, and it grows from 2.08% (at $AR = 0\%$) to 32.46% (at $AR = 80\%$) in US Backbone. However, the power savings in De-EDPC compared with NEDPC does not show the same trend in the two networks. It maintains between 25% and 33% in NSFNET network while it increases a little from 8% to 28% in US Backbone network.

Fig. 9(c) shows the total number of FSs usage. We can see the similar trend in NSFNET and US Backbone networks. Specifically, more FSs are required at a bigger AR for all the p-cycle schemes De-EDPC, EUPC and NEDPC. In addition, EUPC still consumes the most FSs because extra protection capacity is allocated for the asymmetric traffic while NEDPC requires the least owing to the optimization of FSs usage. The FSs usage in De-EDPC is much lower than in EUPC due to the consciousness of the different traffic volumes in the two directions.

D. Impact of DCs Number on Power Savings in De-EDPC

We further investigate the power savings in De-EDPC as a function of the number of DCs. The traffic is generated by setting $AR = 80\%$ and $TASY = 80\%$ so that the impact of number of DCs can be analyzed effectively. The number and location of DCs selected in the simulations are shown in Table IX, which is referred from [25].

Fig. 10 shows the power consumption and FSs usage in De-EDPC, NEDPC and EUPC. From Fig. 10(a) and (b), we

TABLE IX
DCS LOCATION IN NSFNET AND US BACKBONE NETWORKS

Networks	No. of DCs	Location of DCs
NSFNET	1	Node 8
	3	Nodes 1, 8, 14
	5	Nodes 1, 5, 8, 11, 14
	7	Nodes 1, 4, 5, 8, 9, 11, 14
US Backbone	4	Nodes 1, 12, 21, 28
	6	Nodes 1, 7, 14, 19, 21, 28
	8	Nodes 1, 7, 9, 12, 14, 19, 21, 28
	10	Nodes 1, 3, 7, 9, 12, 14, 19, 21, 24, 28

can see that the total power consumption does not show some trend in De-EDPC, NEDPC and EUPC with the increase of the number of DCs. However, compared with EUPC, the introduction of DCs brings the benefit of power savings in De-EDPC since it increases significantly from 6.5% to 46.1% in NSFNET network and from 2.1% to 38.5% in US Backbone network. This is because anycast services in DCs bring asymmetric traffic in the network, then directed p-cycles in De-EDPC consume lower power. Nevertheless, as the number of DCs increases, the power savings in De-EDPC do not change too much even though the amount of power consumption varies in De-EDPC, NEDPC and EUPC, respectively. This is because the asymmetric traffic are set with fixed AR and $TASY$. Compared

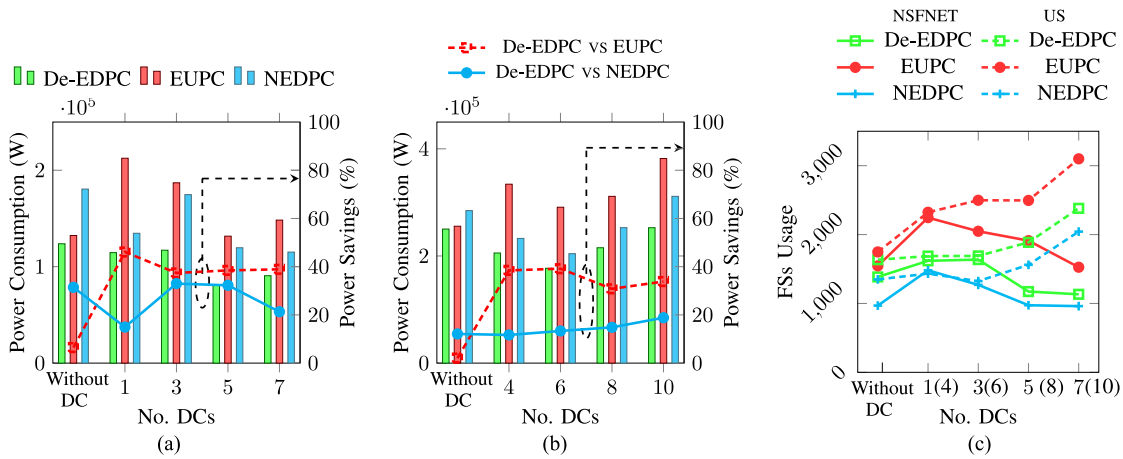

Fig. 10. Power consumption and total FSs usage as a function of the number of DCs. (a) Power consumption and power savings in De-EDPC in NSFNET network. (b) Power consumption and power savings in De-EDPC in US Backbone network. (c) Total FSs usage in NSFNET and US Backbone networks.

with NEDPC, power savings in De-EDPC shows different trends in NSFNET and US Backbone networks. It fluctuates with the increase of the number of DCs in NSFNET while it grows stably in US Backbone network.

The total FSs usage in Fig. 10(c) shows more differences in NSFNET and US Backbone networks. As we can see that in NSFNET network, the total FSs usage goes down with the increase of the number of DCs in De-EDPC, EUPC and NEDPC while it goes up in US Backbone network. However, it is still observed that EUPC requires the most FSs usage while NEDPC needs the least.

Comprehensive simulations of power consumption and FSs usage are preformed in De-EDPC, EUPC and NEDPC for asymmetric traffic in terms of $TASY$, AR and the number of DCs. The results demonstrate that directed p-cycles in De-EDPC own significant power savings (up to 46.91%) compared with undirected p-cycles in EUPC, and the amount of power savings increases with the increase of $TASY$ or AR. In addition, De-EDPC also earns power savings compared with NEDPC, but the amount of power savings does not change too much as the $TASY$ or AR increases. It is also reserved that the introduction of DCs makes it more valuable to utilize directed p-cycles for protection in EONs in a power-efficient way.

VII. Conclusion

Asymmetric traffic provisioning has been proved to be more efficient for new asymmetric services in EONs. This paper studies power-efficient directed p-cycle protection for asymmetric traffic in EONs. Directed p-cycles enable to allocate different spectrum slots and modulation formats for asymmetric traffic in each direction with the help of distinguishing traffic amount in two directions. Simulation results demonstrate that significant power savings are obtained by using directed p-cycles for asymmetric traffic protection in EONs, and the amount of power savings goes up as the $TASY$ or AR increases. In addition, it shows that the introduction of DCs makes it more valuable to utilize directed p-cycles in order to power-efficiently protect the anycast services while the amount of power savings with directed p-cycles does not depend on the number of DCs.

References

[1] M. Ju, F. Zhou, S. Xiao, and Z. Zhu, "Energy-efficient protection with directed p-cycles for asymmetric traffic in elastic optical networks," in *Proc. Eur. Conf. Netw. Opt.*, Jun. 2016, pp. 1–6.

[2] M. Jinno, H. Takara, B. Kozicki, Y. Tsukishima, Y. Sone, and S. Matsuoka, "Spectrum-efficient and scalable elastic optical path network: Architecture, benefits, and enabling technologies," *IEEE Commun. Mag.*, vol. 47, no. 11, pp. 66–73, Nov. 2009.

[3] G. Shen, H. Guo, and S. Bose, "Survivable elastic optical networks: Survey and perspective (invited)," *Photon. Netw. Commun.*, vol. 31, pp. 71–87, Jul. 2015.

[4] Y. Ye *et al.*, "Energy-efficient resilient optical networks: Challenges and trade-offs," *IEEE Commun. Mag.*, vol. 53, no. 2, pp. 144–150, Feb. 2015.

[5] X. Chen, S. Zhu, L. Jiang, and Z. Zhu, "On spectrum efficient failure-independent path protection p-cycle design in elastic optical networks," *J. Lightw. Technol.*, vol. 33, no. 17, pp. 3719–3729, Sep. 2015.

[6] Y. Wei, K. Xu, Y. Jiang, H. Zhao, and G. Shen, "Optimal design for p-cycle-protected elastic optical networks," *Photon. Netw. Commun.*, vol. 29, no. 3, pp. 257–268, 2015.

[7] F. Ji, X. Chen, W. Lu, J. Rodrigues, and Z. Zhu, "Dynamic p-cycle protection in spectrum-sliced elastic optical networks," *J. Lightw. Technol.*, vol. 32, no. 6, pp. 1190–1199, Mar. 2014.

[8] X. Chen, F. Ji, and Z. Zhu, "Service availability oriented p-cycle protection design in elastic optical networks," *J. Opt. Commun. Netw.*, vol. 6, no. 10, pp. 901–910, Oct. 2014.

[9] J. Wu, Y. Liu, C. Yu, and Y. Wu, "Survivable routing and spectrum allocation algorithm based on p-cycle protection in elastic optical networks," *J. Light Electron Opt.*, vol. 125, no. 16, pp. 4446–4451, 2014.

[10] J. L. Vizcaíno *et al.*, "Protection in optical transport networks with fixed and flexible grid: Cost and energy efficiency evaluation," *Opt. Switching Netw.*, vol. 11, pp. 55–71, 2014.

[11] K. Walkowiak, R. Goscien, and M. Klinkowski, "Evaluation of impact of traffic asymmetry on performance of elastic optical networks," in *Proc. Opt. Fiber Commun. Conf.*, Mar. 2015, pp. 1–3.

[12] K. Walkowiak, "Anycasting in connection-oriented computer networks: Models, algorithms and results," *Int. J. Appl. Math. Comput. Sci.*, vol. 20, no. 1, pp. 207–220, 2010.

[13] W. Grover and D. Stamatelakis, "Cycle-oriented distributed preconfiguration: Ring-like speed with mesh-like capacity for self-planning network restoration," in *Proc. IEEE Int. Conf. Commun.*, Jun. 1998, pp. 537–543.

[14] M. Ju, F. Zhou, Z. Zhu, and S. Xiao, "Distance-adaptive, low CAPEX cost p-cycle design without candidate cycle enumeration in mixed-line-rate optical networks," *J. Lightw. Technol.*, vol. 34, no. 11, pp. 2663–2676, 2016.

[15] J. López *et al.*, "Traffic and power-aware protection scheme in elastic optical networks," in *Proc. Telecommun. Netw. Strategy Planning Symp.*, Oct. 2012, pp. 1–6.

[16] J. López *et al.*, "Differentiated quality of protection to improve energy efficiency of survivable optical transport networks," in *Proc. Opt. Fiber Commun. Conf.*, Mar. 2013, pp. 1–3.
[17] N. G. Anoh, J. C. Adépo, M. Babri, and B. Aka, "Hybrid protection scheme for elastic optical networks with regenerator and efficient energy consideration," *J. Computer Sci. Telecommun.*, vol. 6, no. 10, Nov. 2015.
[18] K. Walkowiak, M. Klinkowski, R. Goscien, and A. Kasprzak, "Multiflow transponders for provisioning of asymmetric traffic in elastic optical networks with dedicated path protection," in *Proc. Eur. Conf. Opt. Commun.*, Sep. 2014, pp. 1–3.
[19] R. Goścień, K. Walkowiak, and M. Klinkowski, "Tabu search algorithm for routing, modulation and spectrum allocation in elastic optical network with anycast and unicast traffic," *Comput. Netw.*, vol. 79, pp. 148–165, Jan. 2015.
[20] R. Goścień, K. Walkowiak, and M. Klinkowski, "Joint anycast and unicast routing and spectrum allocation with dedicated path protection in elastic optical networks," in *Proc. Design Rel. Commun. Netw.*, Apr. 2014, pp. 1–8.
[21] D. Zhou and S. Subramaniam, "Survivability in optical networks," *Network*, vol. 14, no. 6, pp. 16–23, Nov. 2000.
[22] H. Wensheng, "Survivable design in WDM mesh networks," in Ph.D. dissertation, Retrospective Theses Dissertations, Dept. Electr. Comput. Eng., Iowa State Univ., Ames, IA, USA, 2006.
[23] S. Ramamurthy, L. Sahasrabuddhe, and B. Mukherjee, "Survivable WDM mesh networks," *J. Lightw. Technol.*, vol. 21, no. 4, pp. 870–883, Apr. 2003.
[24] C. Rocha and B. Jaumard, "Directed vs. undirected p-cycles and FIPP p-cycles," in *Proc. Int. Netw. Optim. Conf.*, Apr. 2009.
[25] X. Dong, T. El-Gorashi, and J. Elmirghani, "On the energy efficiency of physical topology design for IP over WDM networks," *J. Lightw. Technol.*, vol. 30, no. 12, pp. 1931–1942, Jun. 2012.
[26] L. Zhang, W. Lu, X. Zhou, and Z. Zhu, "Dynamic RMSA in spectrum-sliced elastic optical networks for high-throughput service provisioning," in *Proc. Int. Conf. Comput. Netw. Commun.*, Jan. 2013, pp. 380–384.
[27] A. Kodian, A. Sack, and W. D. Grover, "The threshold hop-limit effect in p-cycles: Comparing hop- and circumference-limited design," *Opt. Switching Netw.*, vol. 2, no. 2, pp. 72–85, Sep. 2005.
[28] A. Eshoul and H. Mouftah, "Survivability approaches using p-cycles in WDM mesh networks under static traffic," *IEEE/ACM Trans. Netw.*, vol. 17, no. 2, pp. 671–683, Apr. 2009.
[29] L. Gong, X. Zhou, X. Liu, W. Zhao, W. Lu, and Z. Zhu, "Efficient resource allocation for all-optical multicasting over spectrum-sliced elastic optical networks," *J. Opt. Commun. Netw.*, vol. 5, no. 8, pp. 836–847, Aug. 2013.

Min Ju received the B.S. degree from the University of Electronic Science and Technology of China, Chengdu, China, in 2012. She is currently working toward the joint Ph.D. degree from Shanghai Jiao Tong University, Shanghai, China, and the University of Avignon, Avignon, France.

Fen Zhou received the Ph.D. degree in computer science from INSA Rennes, Rennes, France, in 2010. He is currently an Associate Professor at the Computer Science Lab (LIA), University of Avignon, Avignon, France. His research interests include routing optimization and resource allocation in optical networks, content delivery networks, and vehicular networks.

Shilin Xiao received the M.S. degree from the University of Electronic Science and Technology of China, Chengdu, China, in 1988, and the Ph.D. degree from Shanghai Jiao Tong University (SJTU), Shanghai, China, in 2003. From 1988 to 1999, he worked with the Guilin Institute of Optical Communications. Since 2000, he has ben working with the State Key Laboratory of Advanced Optical Communication Systems and Network, SJTU. His major research interests include optical communications, especially optical switching and passive optical networks. He has published more than 100 papers in technical journals and conferences. He is currently a Professor at SJTU, and a Senior Member of the Chinese Institute of Electronics and the Optical Society of China.

Zuqing Zhu received the Ph.D. degree from the Department of Electrical and Computer Engineering, University of California, Davis, Davis, CA, USA, in 2007. From July 2007 to January 2011, he worked in the Service Provider Technology Group, Cisco Systems, San Jose, CA, USA, as a Senior Engineer. In January 2011, he joined USTC, where he is currently a Full Professor. He has published more than 150 papers in peer-reviewed journals and conferences. He is an Editorial Board Member of IEEE COMMUNICATIONS MAGAZINE, *Journal of Optical Switching and Networking* (Elsevier), *Telecommunication Systems Journal* (Springer), *Photonic Network Communications* (Springer), and others. He has also served as a Guest Editor for IEEE COMMUNICATIONS MAGAZINE and IEEE NETWORK. He has received Best Paper Awards from IEEE ICC 2013, IEEE GLOBECOM 2013, IEEE ICNC 2014, and IEEE ICC 2015. He is a Senior Member of OSA.